foundations

MDPI

Article

Fatty Acid Vesicles as Hard UV-C Shields for Early Life

Iván Lechuga [1] and Karo Michaelian [2,*]

[1] Postgraduate Studies in Physical Science, Universidad Nacional Autónoma de México, Circuito Interior de la Investigación Científica, Cuidad Universitaria, Cuidad de México C.P. 04510, Mexico
[2] Department of Nuclear Physics and Application of Radiation, Instituto de Física, Universidad Nacional Autónoma de México, Circuito Interior de la Investigación Científica, Cuidad Universitaria, Cuidad de México C.P. 04510, Mexico
* Correspondence: karo@fisica.unam.mx

Abstract: Theories on life's origin generally acknowledge the advantage of a semi-permeable vesicle (protocell) for enhancing the chemical reaction–diffusion processes involved in abiogenesis. However, more and more evidence indicates that the origin of life is concerned with the photo-chemical dissipative structuring of the fundamental molecules under soft UV-C light (245–275 nm). In this paper, we analyze the Mie UV scattering properties of such a vesicle created with long-chain fatty acids. We find that the vesicle could have provided early life with a shield from the faint but destructive hard UV-C ionizing light (180–210 nm) that probably bathed Earth's surface from before the origin of life and at least until 1200 million years after, until the formation of a protective ozone layer as a result of the evolution of oxygenic photosynthesis.

Keywords: ultraviolet shield; protocell; fatty acid vesicles; origin of life; dissipative structuring; prebiotic chemistry; abiogenesis; non-equilibrium thermodynamics; thermodynamic dissipation theory; Mie scattering

MSC: 92C05; 92C15; 92C40; 92C45; 80Axx; 82Cxx; 82B35; 82C26

Citation: Lechuga, I.; Michaelian, K. Fatty Acid Vesicles as Hard UV-C Shields for Early Life. *Foundations* **2023**, *3*, 99–114. https://doi.org/10.3390/foundations3010010

Academic Editor: Cristina Achim

Received: 31 December 2022
Revised: 7 February 2023
Accepted: 20 February 2023
Published: 23 February 2023

1. Introduction

The physical and chemical properties of vesicles with walls made from amphiphilic molecules such as fatty acids, isoprenes, and phospholipids have been analyzed in detail in relation to their utility as micro-environments for enhancing reaction–diffusion processes occurring in prebiotic cells at the origin of life [1–4]. Amphiphilic membranes play a role in energy transduction, ion transport, and concentrating molecules, thereby increasing reaction rates [2]. The membrane also allows for the regulated exchange of incoming and outgoing material [5,6] leading to the formation of gradients, which can be useful as energy sources in themselves [7].

However, more and more evidence indicates that the origin of life is concerned with not only chemical reactions (thermally or catalytically activated) but also photochemical reactions [8,9], including UV selection processes [10,11]. In particular, it has been hypothesized that the fundamental molecules of life were formed through dissipative structuring from precursors under the surface UV-C light environment of the early Archean [5,12–16]. The dissipative structuring of organic molecules under light is thus assumed to be the fundamental creative force in biology, from the initial direct dissipative structuring at the UV-C wavelengths of the early Archean leading to the fundamental molecules of life (UV-C pigments), to the dissipative structuring at visible wavelengths up to the red edge (∼700 nm) of the organic pigments of today in the visible. The simultaneous coupling of the organic pigment photon dissipative process with abiotic irreversible processes, such as the water cycle and ocean and air currents, further increases the efficacy of solar photon dissipation into the far infrared, culminating in an efficient global dissipating system known as the biosphere.

Assuming such a dissipative scenario for the evolutionary history of life, it would be important to understand how the optical properties of the vesicle could have affected the UV-C photochemical dissipative structuring of the fundamental molecules at the origin of life. This paper presents a first (as far as the authors are aware) analysis of the optical properties of such vesicles at UV-C wavelengths and how these properties may have influenced the molecular dissipative structuring processes.

In this paper, we investigate the optical properties of pre-biotic fatty acid vesicles given the physical–chemical properties that would have been required for vesicle stability under the ambient conditions of Earth's early Archean ocean surface. Specifically, we determine the vesicle wavelength-dependent absorption and scattering given the requirements of stability against high temperature, pH variation, and salt flocculation. In particular, we analyze the possibility that vesicles could have acted as Mie scattering particles for the high energy ionizing UV-C photons in the 180–210 nm region (labeled here as "hard" UV-C photons), thereby preventing damage to the fundamental molecules of life, which we assume were dissipatively structured within the vesicle with generally "soft" UV-C photons (defined here as having wavelengths between 245 and 275 nm). We find that an important protective effect against hard UV-C photons indeed occurs for specific vesicle radii that, interestingly, are concordant with the size distribution of the oldest cyanobacteria found in the Archean fossil record at 3.49, 3.45, and 3.2 Ga [17].

Furthermore, we suggest that, as a result of UV-C light back-scattering from vesicles, followed by total internal reflection at the ocean surface, vesicles could thereby increase the amount of circularly polarized UV-C light available to the molecules confined within neighboring vesicles. This has relevance to the origin of life since we have proposed elsewhere [18,19] that the homochirality of life arose from the DNA or RNA UV-C photon-induced denaturing resulting from the dissipation of these soft UV-C photons in double-strand DNA and RNA, in conjunction with the asymmetry in this light-induced denaturing due to the small morning/afternoon temperature difference (∼4 °C today) of the ocean surface.

2. The Thermodynamic Dissipation Theory for the Origin and Evolution of Life

The dissipative structuring of material under an externally imposed generalized thermodynamic potential is a well-established non-equilibrium thermodynamic result which leads to the complexation of physical–chemical systems in such a manner as to increase the dissipation of the imposed potential [20]. The Thermodynamic Dissipation Theory for the Origin and Evolution of Life [5,12–14,16,18,19,21] identifies this generalized thermodynamic potential for the dissipative structuring involved in the origin of life as the solar photon potential of UV-C wavelengths between 205 and 285 nm. In this region, photons can break and remake covalent bonds in carbon-based molecules but rarely cause molecular dissociation through ionization. This photon potential was available at the Earth's surface before the origin of life (∼3.9 Ga) and persisted for at least 1200 million years until the emergence of oxygenic photosynthesis and an ensuing ozone layer at about 2.7 Ga [10,22].

The thermodynamic dissipation theory for the origin of life proposes that the fundamental molecules of life (those in the three domains of life—nucleic acids, amino acids, fatty acids, sugars, cofactors, etc.) were initially UV-C pigments [14] dissipatively structured on the ocean surface from common precursors such as HCN, cyanogen, CO_2, and water under the UV-C photon potential [5,16,21,23]. It is assumed that the prebiotic vesicles would form from these dissipatively structured fatty acids [21] and isoprenes at the ocean surface, through surface agitation and natural Gibb's free energy minimization.

Although, from the photochemical dissipative structuring perspective presented here, an ocean surface origin of life would be favored over a hydrothermal vent scenario because of greater molecular stability and greater available surface area, our results may also be relevant to the hypothesis of an origin of life at the terrestrial hydrothermal fields associated with volcanic land masses exposed to solar UV-C light. In this case, wetting and drying

cycles coupled to photochemical reactions [16,24] could have fomented polymer synthesis within vesicles [25,26].

3. Physical, Chemical, and Optical Properties of Archean Vesicles

3.1. Properties of Fatty Acid Vesicles at the Origin of Life

Natural fatty acids are formed from a carboxyl head group with a hydrocarbon tail of from 4 to 40 carbon atoms [27]. The empirical evidence indicates that the earliest ancestors of the modern cellular membranes were devoid of the relatively more complex phospholipids [28,29]. Furthermore, simple fatty acids are easily produced as small chains of ethylene (C_2H_4) through activated Fischer–Tropsch, or soft UV-C photochemical, polymerization [21]. Ethylene itself can be produced from the reduction of CO_2 or CO in water, or from the UV photolysis of methane [21]. Today, fatty acids are found in the membranes of the cell walls of organisms from all three domains of life [29].

From the perspective of the thermodynamic dissipation theory for the origin of life, we have suggested that conjugated fatty acids of about 18 carbon atoms were prominent among the fatty acids that formed the first prebiotic vesicles [21]. Vesicles made from fatty acids of these lengths are stable at the high temperature of the early Archean surface (~85 °C [30,31]). The critical vesicle concentration (CVC) of these fatty acids required for vesicle formation decreases as the alkyl chain length increases, since longer chains favor the increased packing of bilayers. Triple conjugated forms of these fatty acids absorb strongly near 260 nm, which is at the peak of the UV-C surface photon spectrum available throughout the Archean (Figure 1).

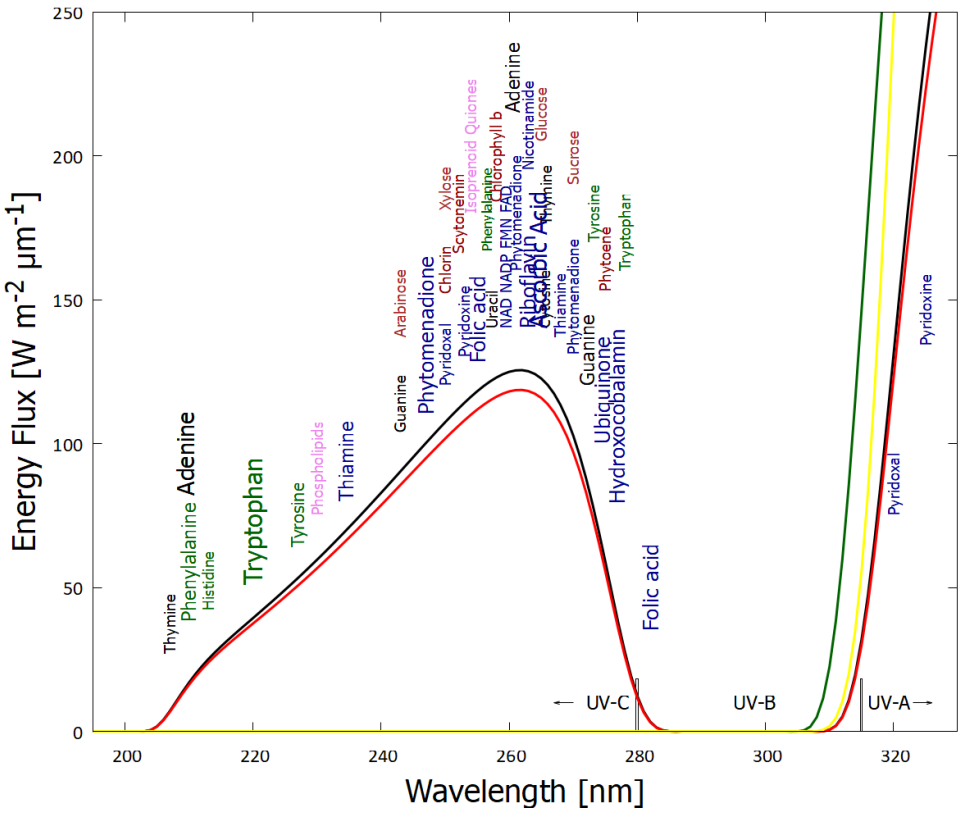

Figure 1. The spectrum of UV light available at the Earth's surface before the origin of life at approximately 3.9 Ga and until at least 2.9 Ga (curves black and red, respectively) (perhaps even extending throughout the entire Archean until 2.5 Ga [32]). Atmospheric CO_2 and perhaps some volcanic H_2S

were responsible for absorption at wavelengths shorter than ∼205 nm, and atmospheric aldehydes (common photochemical products of CO_2 and water) absorbed between about 285 and 310 nm [10], approximately corresponding to the UV-B region. Around 2.2 Ga (green curve), UV-C light at Earth's surface was completely extinguished by oxygen and ozone resulting from organisms performing oxygenic photosynthesis. The yellow curve corresponds to the present-day surface spectrum. Energy fluxes are for the sun at the zenith. The names of the fundamental molecules of life are plotted at their wavelengths of maximum absorption; nucleic acids (black), amino acids (green), fatty acids (violet), sugars (brown), vitamins, co-enzymes and cofactors (blue), and pigments (red) (the font size roughly corresponds to the relative size of their molar extinction coefficient). Adapted from [14].

Indeed, the evidence in the Archean fossil record, and also in modern oceans, shows a predominance of fatty acids with an even number of carbon atoms, particularly a predominance of 16 and 18 carbon atoms [33,34]. The ubiquity of chains with an even number of carbon atoms could be explained if the early Archean fatty acids were formed through the polymerization of ethylene (C_2H_4). In fact, there is a very simple photochemical dissipative structuring route involving the polymerization of ethylene to form fatty acids, starting from CO or CO_2 saturated water [21,35].

The melting temperature of vesicle generally increases with the fatty acid carbon tail length and the degree of hydrogen saturation, with the greater influence being due to saturation. Long chain fatty acids that are partially unsaturated (and therefore conjugated) could form stable vesicles at the high temperatures of the early Archean. For example, fully conjugated (triple) linolenic acid (cis-9, cis-12, and cis-15 18:3) has a strong and wide absorption band at 269 nm and a vesicle melting temperature of around 85 °C (the Earth's average surface temperature as obtained from isotopic evidence in sediments dating back to the origin of life [30,31]).

3.2. Photochemical Dissipative Structuring of Fatty Acids

We have suggested that the formation of fatty acids was most likely through soft UV-C photochemical dissipative structuring in CO_2 saturated water at the ocean surface, leading to ethylene and its polymerization [16,21]. In support of this suggestion is the fact that the polymerization rates of ethylene are two orders of magnitude greater at 254 nm (UV-C) than at 365 nm (UV-A) [36].

Another possible photo-induced route to fatty acids synthesis in the UV-C and UV-B regions starts with formaldehyde under this light and ZnO and TiO_2 acting as photocatalysts, leading to the formation of from two to five carbon fatty acids, as well as to other fundamental molecules of life [37]. For example, the route to fatty acid formation includes the oligomerization of HCN into diaminomaleonitrile DAMN, which can proceed through photon absorption in the UV-C region between 205 and 285 nm, similar to the photochemical dissipative structuring routes of the purines proposed elsewhere by the authors [5,6].

It is known that saturated (non-conjugated) fatty acids absorb very little in the UV-C region, except for dissociation below ∼180 nm and a small absorption peak from the carboxyl head group at 207 nm [38]. UV-C light between 205 and 285 nm can, however, induce the de-protonation of fatty acids leading to the conjugation of carbon bonds in the acyl tail [39]. After several deprotonation events and migration of the double bonds, the fatty acids arrive at a conjugated configuration; diene for two double bonds with absorption at 233 nm, triene for three double bonds with absorption at 269 nm, and tetraene for those with four double bonds providing absorption at 310–340 nm. All these wavelengths lie within the likely Earth's Archean surface photon spectrum (Figure 1). Furthermore, conjugated fatty acids have conical intersections [40] allowing for the rapid (sub-picosecond) dissipation of the photon-induced excited state energy into heat, which is yet another strong indication of their production at the origin of life through UV-C dissipative structuring [5,16].

The same UV-C photons can also induce cross-linking between adjacent tails of fatty acids at the site of double bonds, resulting in a reduction in the average conjugation number [41]. A stationary state distribution of the fatty acid conjugation number, with a

maximum at triple conjugation (providing absorption at 269 nm, near the peak in the UV-C surface spectrum—Figure 1), would thus arise under the constant UV-C flux [21].

The steps involved in the dissipative structuring of fatty acids can thus be summarized as follows [21]; (i) UV-C-induced reduction of CO_2 or CO in water saturated with these, forming ethylene, (ii) UV-C-induced polymerization of ethylene to form long hydrocarbon tails of an even number of carbon atoms (e.g., 18 C), (iii) oxidation and hydrolysis events to stop the growth of the chain and form the carboxyl head group, respectively, (iv) UV-C induced deprotonation of the tails to form double carbon–carbon bonds, and (v) double bond migration to provide a conjugated diene, triene, or tetraene molecule with a conical intersection. The conical intersection provides the sub-picosecond decay of the electronic excited state energy into harmless heat, preventing further photochemical reactions and, thus, providing photochemical stability and, most importantly, from our perspective of dissipative structuring, photon dissipative efficacy.

4. Model

When electromagnetic radiation impinges on a particle in-bedded in a medium, the particle's material polarizes. The induced dipoles oscillate with the incoming radiation and produce a new electromagnetic field, known as the scattered field. The incoming light may also be absorbed by the particle material. Thus, the particle has both a real and imaginary refractive index. Our fatty acid vesicle is such a particle in-bedded in ocean surface water with sunlight incident from above (Figure 2). The vesicle is assumed to be spherical, with a core consisting of DNA, RNA, and other fundamental molecules in a water solution, covered by a mantle consisting of a bi-layer membrane of ∼18-carbon atom fatty acids (a size for which there is a peak concentration of fossils found in Archean sediments [33,34]).

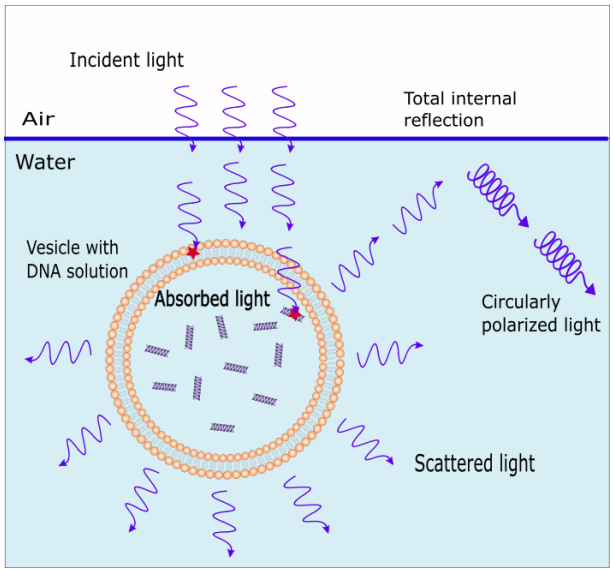

Figure 2. Scattered and absorbed light by a fatty acids vesicle. Light from the sun travels through a thin layer of ocean water and interacts with the vesicle. Some of the light is absorbed by the fatty acid vesicle wall and the DNA, RNA, and other fundamental molecules assumed to have been dissipatively structured within the vesicle. Another part of the light is scattered, mainly in the forward direction. The scattered light is plane polarized and some of it may then be totally internally reflected at the ocean surface, producing circularly polarized light that may have been important in engendering the homochirality of life [18].

The problems associated with fatty acids vesicle formation and stability are; (1) the narrow range of alkaline pH in which vesicles spontaneously form [42], (2) salt flocculation (agglomeration at high salt concentrations) [43,44], and (3) high critical vesiculation concentration (critical concentration of fatty acids required for spontaneous vesicle formation), higher than, for example, the equivalent for phospholipid vesicle formation [1,45].

The limited pH stability and salt flocculation can be improved through the covalent cross-linking of neighboring chains of fatty acids, which could have been induced by either UV-C light, temperatures above 50 °C, simple aging, or any combination of these [41,45]. A structure of side-by-side overlap of chains of the two layers of the bilayer vesicle, with an overlap of double bonds, provides further stability over an even wider pH range (2–14) [1]. This side-by-side structure enhances the likelihood of cross-linking by all three mechanisms mentioned.

Another possible fatty acid for our vesicle could be the aromatic 12-phenyldodecanoic acid, also of 18 carbon atoms. In this case, the aromatic rings of the two different layers in the bi-layer wall could overlap, providing greater stability at the high temperature, salt, and lower pH values of the Archean ocean surface (UV-C light, ∼85 °C, salt 1.5 to 2 × today's value, pH∼6.5 [31]). Indeed, the aromatic ω-phenyl fatty acids 10-phenyltridecanoic acid (16 carbon atoms), 12-phenyldodecanoic acid (18 carbon atoms), and 14-phenyltetradecanoic acid (20 carbon atoms) are found in the highly salt resistant marine bacteria V. alginolyticus [46], and ω-cyclohexyl fatty acids are found today in some acidophilic–thermophilic bacteria isolated from hot springs [47].

Considering these light, temperature, salt, and pH conditions of the early Archean ocean surface, vesicles with a bilayer constituted of 18-carbon atom fatty acids such as 12-phenyldodecanoic acid or linolenic acid with cross-linking between them, could be expected to have been floating near the surface. For the lack of published UV-C absorption data for these two fatty acids, our model assumes the UV-C absorption coefficient of cinnamic acid [48] as a proxy for 12-phenyldodecanoic acid, since the only difference is in the length of the hydrocarbon chain. The error introduced by choosing whatever particular fatty acid would not be large, however, since the vesicle wall contributes little to the scattering and absorption due to its thinness with respect to the vesicle size.

5. Method

The efficiencies Q of extinction, scattering, and absorption (extinction minus scattering) are defined as the ratio of the observed cross-sections to the geometrical cross-section, which, for a spherical vesicle of radius a, is πa^2 [49]. We employed the BHCOAT code [49] to compute the extinction efficiency, Q_{ext}, the scattering efficiency, Q_{sca}, the absorption efficiency, Q_{abs}, and the backscattering efficiency, Q_{back}, for the vesicle for unpolarized light. The computation assumes Mie theory, valid for vesicles larger than the incident wavelengths.

The input to the BHCOAT code for calculating Mie scattering consisted of the incident light wavelength, the radius of the vesicle core, the thickness of the fatty acid membrane (estimated to be 5 nm for a bilayer of 18-carbon atom fatty acids), the real refractive index of the surrounding water medium, and the complex refractive indexes of the fatty acids and the core solution containing DNA, RNA, and other fundamental molecules in water. The real refractive index n for water as a function of wavelength was obtained from the data of Hale and Querry [50]. The real refractive index of the core solution of DNA, RNA, and other fundamental molecules in water depends on the concentration of these molecules (e.g., Figure 5 of [51] shows how the index of refraction increases as a function of the concentration of DNA in the water solution). The experiments by Liu et al. [52] determine an index of refraction n of present day cell nuclei of between 1.353 and 1.367, which corresponds to a scale factor 1.01 and 1.02 times that of pure water at 589 nm ($n = 1.34$). The refractive index of the fatty acid vesicle wall was taken as 1.39 at 589 nm [53]. For the lack of published wavelength-dependent data for the real refractive index of the core solution, and for the fatty acid vesicle wall, we took the wavelength dependence to be the same as that of pure water multiplied by their corresponding scale factor. The results are plotted in Figure 3.

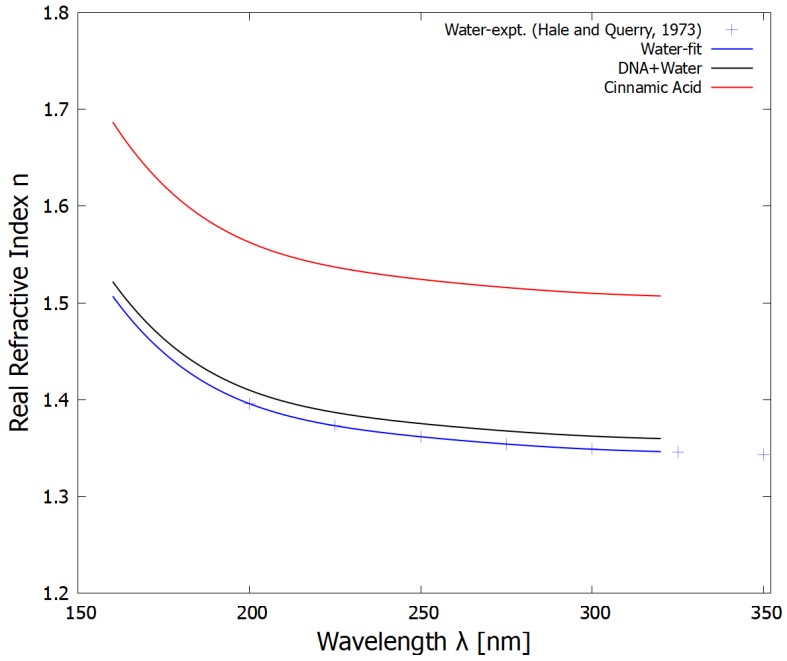

Figure 3. The real part of the refractive indexes for water (blue), the solution of DNA, RNA, and other fundamental molecules in water (black), and the fatty acid bilayer (red) as a function of wavelength. The blue crosses are the experimental data points for water obtained from [50]. The refractive index for the fundamental molecules in water (black line) was obtained by multiplying the refractive index of water by a constant scale factor (see text), either 1.01 (plotted) or 1.02 (not plotted). The real refractive index of the fatty acid vesicle wall was anchored to the experimental value of 1.39 at 589 nm, corresponding to cinnamic acid ($C_9H_8O_2$) [53] (which should be similar to 12-phenyldodecanoic acid since both have aromatic geometry) and given the same wavelength dependence as that of water (oils also present a similar increase in refractive index as the wavelength decreases [54]). In any case, because of the small thickness of the vesicle wall (5 nm) in comparison to the vesicle radius (>1 μm), the refractive index of the vesicle wall, or its wavelength dependence, do not affect the scattering results by any noticeable amount.

The imaginary part of the complex refractive index for water was obtained from the absorption data of Hale and Querry [50] and Chaplin [55] and is plotted as the blue points with the fitted blue curve in Figure 4.

The extinction coefficient k for the solution of the DNA and fundamental molecules in water is also plotted in Figure 4 and depends on the molar extinction coefficient ϵ (obtained from Umazano and Bertolotto [56] for DNA in water) and on the concentration c of the DNA in water (i.e., $k(\lambda) = \frac{\lambda}{4\pi}\epsilon(\lambda) \cdot c$). Since the concentration c comes in as a multiplicative factor, we have applied a scale factor of 10 to the data of Umazano and Bertolotto so that the DNA absorption will be noticeable on Figures 7 and 8 that plot the scattering and absorption together on the same scale. It is the ratio of scattering (and the ratio of absorption) in the different wavelength regions, not the absolute values of these, that is important for our demonstration (see below).

The imaginary part of the refractive index for the 12-phenyldodecanoic acid bilayer wall as a function of wavelength was obtained from the absorption data of the proxy cinnamic acid (both are aromatic fatty acids, the only difference being the length of the hydrocarbon tail) published in the NIST handbook [48] and is plotted as the red data points together with the fitted curve in Figure 4.

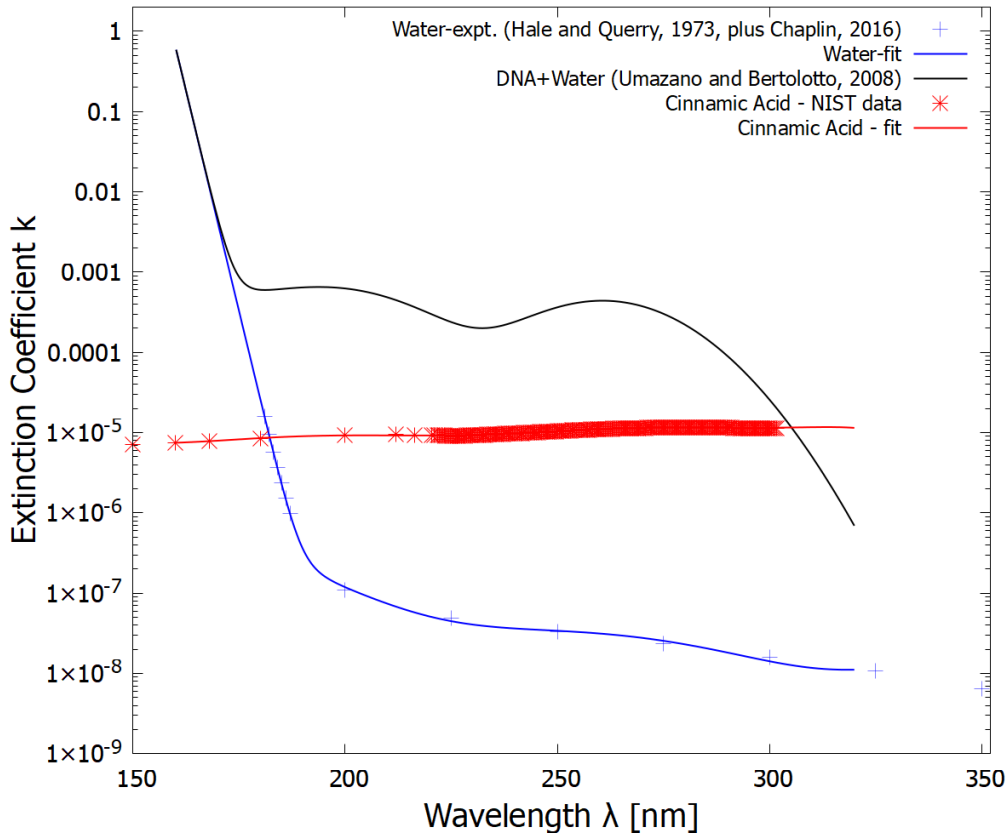

Figure 4. The imaginary part of the refractive indexes for pure water (blue line fit to experimental data of Hale and Querry [50] and Chaplin [55]—crosses), the solution of DNA in water (black line—obtained by multiplying the data from Umazano and Bertolotto [56] by a factor of 10—see text), which represents DNA, RNA, and other fundamental molecules in water solution within the vesicle, and the fatty acid bilayer wall (red line—obtained by fitting to data from the NIST handbook for cinnamic acid [48], similar to 12-phenyldodecanoic acid—see text) as a function of wavelength.

6. Results

6.1. Scattering and Absorption

The efficiencies Q_{ext}, Q_{sca}, and Q_{abs} ($Q_{ext} - Q_{sca}$) were integrated over the soft and hard UV-C wavelength regions (per unit area presented to the photon beam) plotted as a function of vesicle core radius for the case of the core (DNA, fundamental molecules and water) real refractive index of 1.01 times that of pure water in Figure 5. The results show an expected diffraction pattern for small radii. A photo-protective effect against the hard UV-C light is also visible for certain vesicle radii since Q_{sca} is maximum for the integrated region of 180–210 nm (blue curve, Figure 5) when the vesicle core radius is 4.4 μm, with another peak at 11.8 μm. These hard UV-C wavelengths have enough energy to dissociate nucleic acids, amino acids, proteins, and other fundamental molecules of life confined within the vesicle. The shielding by Mie scattering thus protects these fundamental molecules from disassociation allowing them to be efficient at absorbing and dissipating in the soft UV-C (245–275 nm) region (Figure 1). Note, however, that at these small radii, very little of the soft UV-C light is absorbed by the core since most of this light is scattered.

The same scattering and absorption efficiencies for a greater core refractive index of 1.02 times that of pure water are provided in Figure 6. As the refractive index of the core solution increases, the vesicle radius giving greatest scattering (shielding) of the dangerous ionizing radiation (blue line) decreases to the smaller value of 2.2 μm with a lesser peak at 5.9 μm, corresponding to protocell diameters of 4.4 and 11.8 μm, respectively.

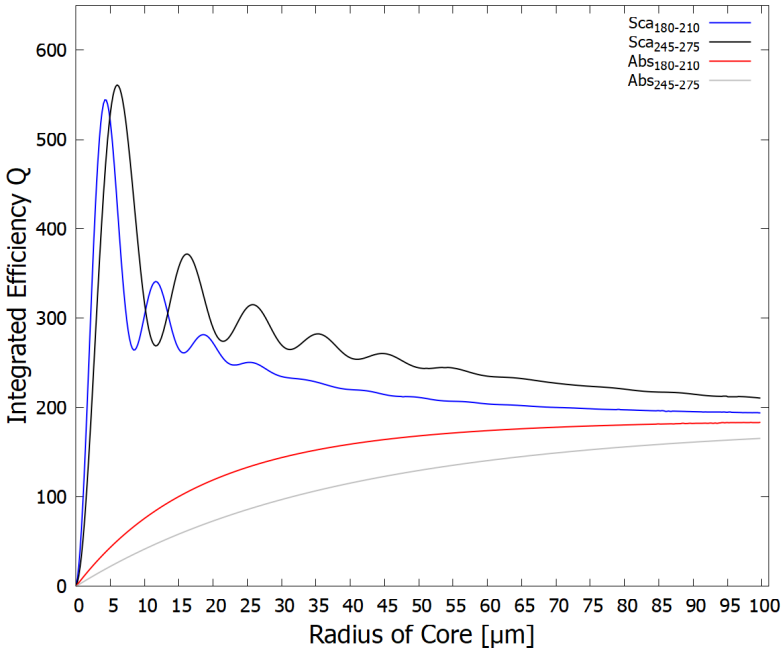

Figure 5. The integrated efficiency of scattering Q_{sca} and absorption Q_{abs} per unit area presented to the light beam of the fatty acid vesicle for two different wavelength regions (180–210 nm—ionizing/disassociation region) and (245–275 nm—dissipative structuring region) as a function of vesicle core radius (the fatty acid vesicle wall has a thickness of 5 nm). The real refractive index of the core (DNA, fundamental molecules and water solution) is taken to be 1.01 times that of pure water (Figure 3). Note that the greatest scattering (shielding) of the dangerous ionizing radiation (blue line) occurs for the vesicle radius of about 4.4 μm with a smaller peak at 11.8 μm, which would correspond to protocells of diameter 8.8 and 23.6 μm, respectively.

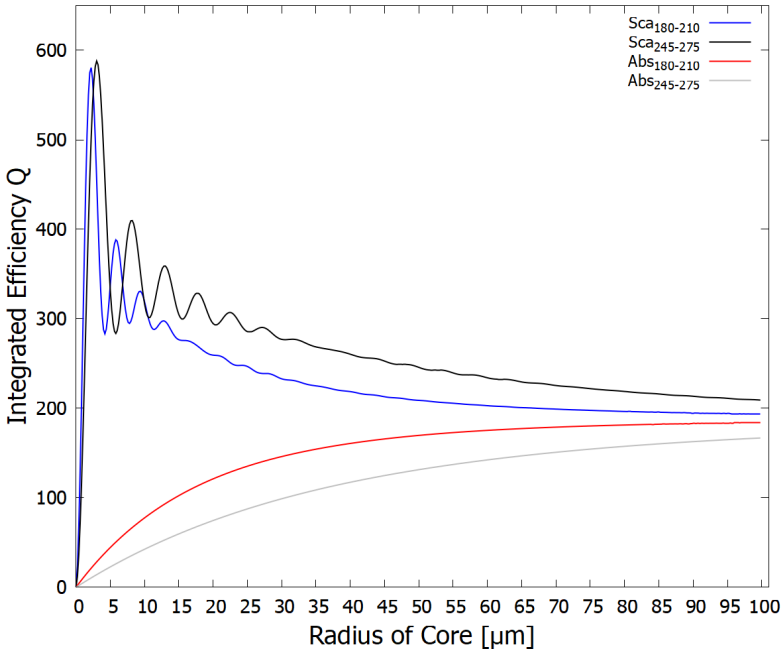

Figure 6. The same as for Figure 5 except using a real refractive index for the core (DNA, fundamental molecules and water solution) of 1.02 (instead of 1.01) times that of pure water. The greatest scattering (shielding) of the dangerous ionizing radiation (blue line) now occurs for a smaller vesicle radius of about 2.2 μm with a smaller peak at 5.9 μm, corresponding to protocell diameters of 4.4 and 11.8 μm, respectively.

In Figures 7 and 8, we plot the wavelength dependence of the extinction, scattering, and absorption efficiencies (observed cross-sections compared to the geometrical cross-section of the vesicle, i.e., πa^2) for vesicles of different radii. The fact that the efficiencies can be greater than 1 (and the fact that there is a diffraction-like pattern at small radii–Figures 5 and 6) results from the fact that photons are not point particles but really quantum waves interacting with the vesicle edge [49]. Figure 7 displays the results for two different vesicle radii of 4.4 and 11.8 μm at which the integrated scattering over the dangerous ionization/disassociation region is maximum (see blue line, Figure 5). For the smaller size of 4.4 μm, the scattering in the dangerous region of from 180 to 210 nm is about 2.8 times greater than that which would be expected classically from the geometrical cross-section. Such vesicle radii would thus be useful, for example, during epochs in which there was lower CO_2 or little H_2S (ejected from volcanoes) in the atmosphere to shield the fundamental molecules from this dangerous radiation (see Figure 1). Note, however, that the absorption (solid red line) in the soft UV-C region (245–275 nm) is quite small since strong scattering in this spectral region also occurs.

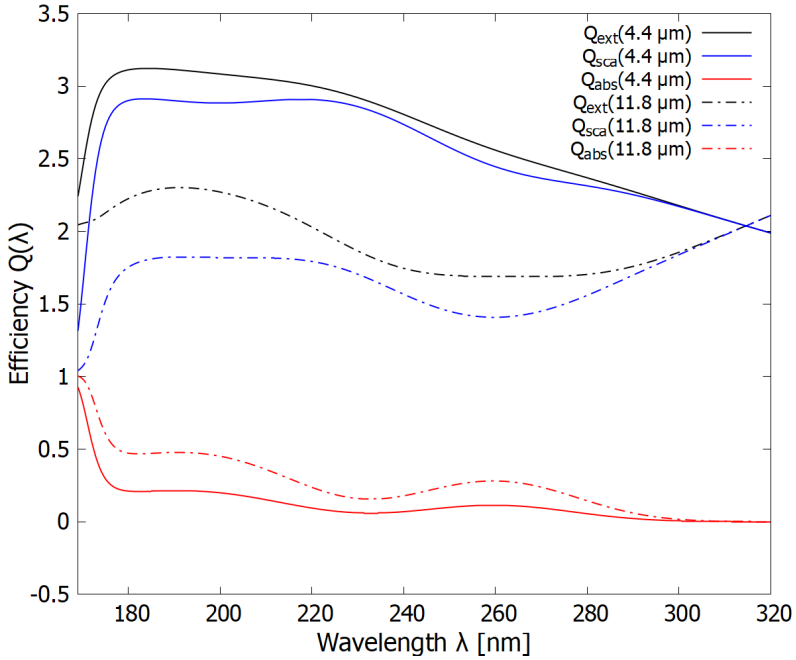

Figure 7. The wavelength dependence of the extinction, scattering, and absorption efficiencies (cross sections compared to the geometrical cross-section of the vesicle) for the real refractive index of the core taken to be 1.01 times that of pure water and a vesicle radius of 4.4 μm (solid lines) and 11.8 μm (dashed lines) providing maximum protection in the dangerous ionization/disassociation region of from 180 to 210 nm (see Figure 5). At the larger radius, the scattering (blue dashed line) protection in the ionizing/disassociation region (180–210 nm) decreases, while absorption (red dashed line) increases in the dissipative structuring region (245–275 nm).

A second, smaller maximum in the scattering of the dangerous hard UV-C photons is observed at a radius of 11.8 μm (Figure 5). The wavelength dependence of this scattering is depicted by the blue dashed line in Figure 7. At these greater radii, less, but still significant, scattering occurs in the dangerous hard UV-C region (about 1.75 times that of the geometrical cross-section) but more light is absorbed in the soft UV-C region that is useful for dissipative structuring.

At the largest radius studied here (100 μm—Figure 8), the scattering and absorption in the hard UV-C region are approximately equal and we find a maximum in the absorption of the soft UV-C photon region. Such vesicle radii would thus be relevant when there was more CO_2 or H_2S in the atmosphere to shield the hard UV-C light, or for vesicles at greater ocean depths.

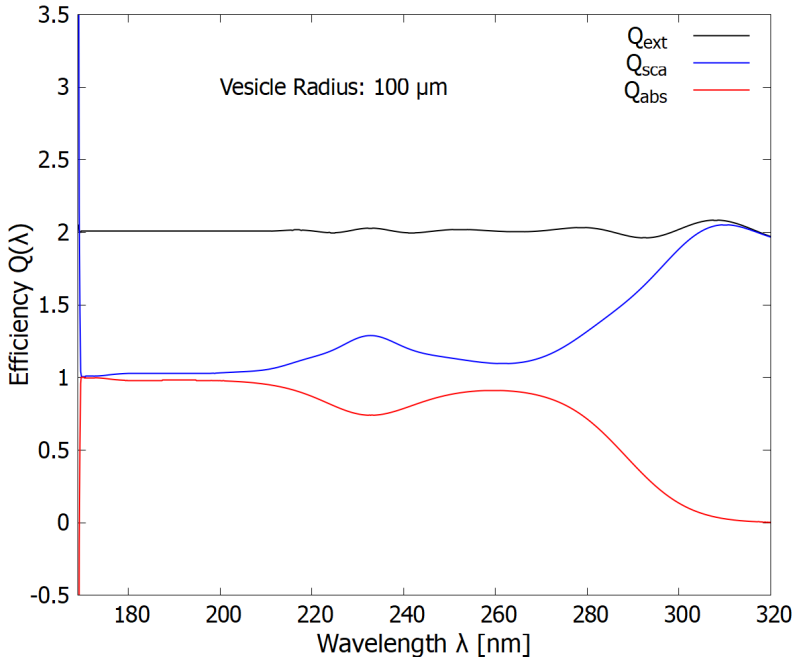

Figure 8. The wavelength dependence of the extinction, scattering, and absorption efficiencies (cross sections compared to the geometrical cross-section of the vesicle) for a vesicle radius of 100 μm (corresponding to the high end of bacteria sizes of today). The Mie scattering (blue line) protection in the ionizing/disassociation region (from 180 to 210 nm) decreases significantly while absorption in the dissipative structuring region (245–275 nm) increases significantly with respect to smaller vesicle radii (Figure 7).

Larger vesicle sizes thus show less protection in the ionization/disassociation region (Figure 8) but more absorption in the soft UV-C region, while certain smaller sizes show greater protection in the ionization/disassociation region but less absorption in the important dissipative structuring region (Figure 7).

From the above figures and discussion, it is apparent that natural thermodynamic selection of the vesicle radius could have occurred, depending on the prevailing light conditions, in order to maximize the dissipative structuring of the fundamental molecules under soft UV-C photons, while simultaneously maximizing the probability of survival of these molecules under the hard UV-C photons. The same optimization could also have been achieved by affecting the concentration of fundamental molecules in the vesicle interior, thereby changing the core refractive index (compare Figures 5 and 6) by, for example, affecting the permeability of the vesicle wall through the incorporation of shorter chain, or conjugated (unsaturated and kinked), fatty acids.

6.2. Backscattering, Optical Dichroism, and Homochirality

A first scattering of light causes an initially unpolarized beam to become linearly polarized. The total internal reflection of this linearly polarized beam at the ocean surface then results in a component of circular polarization (Figure 2). Depending on the direction of observation, the beam is either left- or right-handed circularly polarized [18]. The surface of the ocean is, in fact, known empirically to be the region on Earth with the greatest circular polarization of light, reaching up to 5% of the available submarine light at the ocean surface for low solar angles (early morning or late afternoon) [57].

Left- or right-handed circularly polarized light will both absorb similarly on the vesicle fatty acid wall since fatty acids are not chiral molecules, but this is not the case for the DNA and RNA within the vesicle. We have demonstrated [18] that, given the measured circular dichroism of the nucleic acids and the measured circularly polarized component of light just beneath the ocean surface today, and assuming a similar component during

the Archean, and given the existence of ultraviolet and temperature-assisted denaturing of double-strand DNA or RNA [19], complete 100% homochirality could have been produced in as little as a few thousand Archean years [18].

In Figure 9, we show the integrated backscattering of the soft UV-C photons (245–275 nm) as a function of vesicle radius. Backscattering is greatest at large vesicle radii, as would be expected classically. This backscattered light could then be totally internally reflected from beneath the ocean surface. At the shallower solar angles, of the morning and afternoon, a greater amount of forward scattered light from the vesicles could also be totally internally reflected at the surface, providing a greater component of circular polarization. A considerable amount of light from either backscattering at higher solar angles, or from forward scattering at shallower solar angles, from vesicles at the surface, could have contributed to the formation of homochirality through UV-C and temperature-assisted denaturing [19] in the nucleic acids within neighboring vesicles.

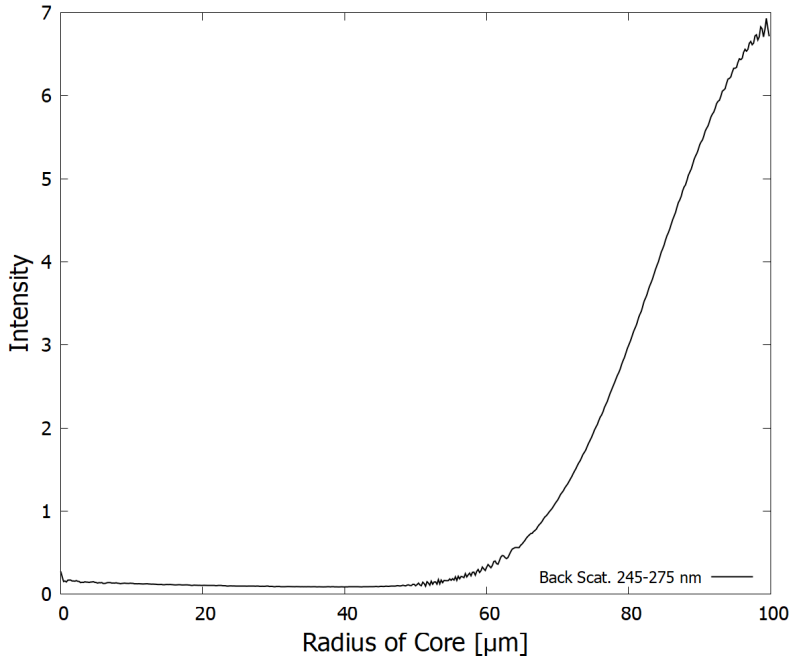

Figure 9. The efficiency of backscattering Q_{back} into a unit solid angle for the fatty acid vesicle for the wavelength region (245–275 nm—dissipative structuring region) as a function of vesicle core radius (the fatty acid mantel has a thickness of 5 nm and the core solution of fundamental molecules and water has a refractive index of 1.01 times that of pure water). For Mie scattering, backscattering is an order of magnitude smaller than forward scattering and is relatively independent of the angle. It increases with size of the vesicle radius. This backscattered light, along with some forward scattered light at low solar angles, if then totally internally reflected at the ocean surface would provide circularly polarized light for inducing the homochirality of the nucleic acids in neighboring vesicles [18,19].

7. Discussion and Conclusions

The thermodynamic dissipation theory for the origin and evolution of life [5,12,13,16,58] proposes that fatty acids and other fundamental molecules of life were dissipatively structured from simple precursors such as HCN and cyanogen on the ocean surface under the Archean UV-C solar light flux. As for all the fundamental molecules of life, these dissipatively structured fatty acids performed the thermodynamic function of dissipating the UV-C photon flux into heat [14]. The evidence for this includes the fact that conjugated fatty acids strongly absorb this light and have conical intersections allowing the photon-induced excitation energy to be rapidly dissipated into heat. Furthermore, the fatty acids are formed through photochemical routes in which incident photon dissipation rates increase with each step of the photochemical reaction process on route to the final product,

which has one or more conical intersections to the ground state. Such photochemical evolution is the hallmark of molecular dissipative structuring [5,16].

In this paper, we looked, for the first time, at the UV-C optical properties of vesicles consisting of a mantle bilayer of fatty acids and an interior core of DNA and other fundamental molecules in water, floating near the ocean surface. In particular, we determined that Mie scattering could have led to some shielding of the damaging hard UV-C photons of the Archean which could cause ionization and disassociation of the fundamental molecules within the core. According to the Mie theory, the maximum scattering of the hard UV-C photons by the vesicle occurs at particular radii that depend on the concentration of the DNA and fundamental molecule solution in the core (i.e., the real refractive index of the core). These sizes, for concentrations of fundamental molecules similar to that of today's cells, are consistent with the sizes of fossil bacteria discovered in sediments of the early Archean period [17] when intense UV-C light was arriving at the Earth's surface. Figures 5 and 6 show that the greater the refractive index of the core with respect to that of the surrounding water, the smaller the radius of the vesicle that provides maximum scattering of the damaging hard UV-C photons.

In our analysis, the wavelength dependence of the real refractive index of the DNA plus fundamental molecule and water vesicle core solution was taken to be the same as that of water multiplied by a constant factor of either 1.01 or 1.02, covering the range of the refractive indexes at 589 nm of present day cells. A better calculation of the refractive index at UV-C wavelengths could be obtained from future experiments or from careful Kramers–Kronig relations given precise wavelength dependent extinction coefficients.

Because of the small thickness of the vesicle wall (5 nm) in comparison to the vesicle radius (>1 μm), the characteristics of the fatty acid constituting the bi-layer, such as the real and imaginary refractive index of the vesicle wall, its wavelength dependence, or its thickness (hydrocarbon tail length) do not affect the scattering or absorption results by any appreciable amount. The bi-layer basically acts as a barrier, separating the two regions of different refractive indexes (i.e., the external ocean water from the solution containing fundamental molecules in the interior of the vesicle).

For concentrations of fundamental molecules similar to those found in modern-day bacteria (providing real refractive indexes about 1.01 times that of pure water), maximum hard UV-C scattering occurs at small vesicle diameters (<24 μm), while maximum absorption of soft UV-C photons occurs at diameters greater than 100 μm. The size of the vesicle could thus have been naturally selected (thermodynamically selected from our perspective) to provide the greatest dissipative structuring with the least amount of molecular disassociation through ionization according to the particular surface UV-C photon spectrum of the epoch (dependent on the pressure of the atmospheric gases CO_2 and H_2S that absorb the hard UV-C photons). For example, the vesicles of independent (unicellular) bacteria have been found in Archean deposits with diameters of less than 24 μm at ∼3.43 Ga, and with diameters of up to 289 μm at ∼3.2 Ga [17].

The backscattering of light with the sun overhead at high angles to the horizon, or forward scattering at low solar angles, of the soft UV-C photons incident on the vesicle could have been totally internally reflected at the ocean surface, thus resulting in an additional component of circularly polarized light that could have induced homochirality in the nucleic acids of neighboring vesicles [18,19].

The results obtained here imply that fatty acid vesicles could indeed have shielded hard UV ionizing radiation from interfering with the molecular dissipative structuring of the fundamental molecules during the Archean. Such dissipative structuring, therefore, may also be viable on the planets of any stars emitting significant UV-C light, even though the planet may not contain sufficient atmospheric CO_2 or hydrogen sulfide during a given epoch to filter out all the high energy ionizing and disassociating photons. This would imply a more robust origin of life, and open up the possibility that carbon-based life as we know it may exist on planets of a much greater number of stars.

Author Contributions: Conceptualization, I.L.; methodology, K.M.; software, K.M. and I.L.; validation, I.L. and K.M.; formal analysis, I.L. and K.M.; investigation, I.L. and K.M.; resources, K.M.; writing—original draft preparation, K.M. and I.L.; writing—review and editing, K.M. and I.L.; visualization, K.M. and I.L.; supervision, K.M.; project administration, K.M.; funding acquisition, K.M. All authors have read and agreed to the published version of the manuscript.

Funding: This research was funded by DGAPA-UNAM, grant number IN104920. I.L. is grateful for a national postgraduate scholarship from CONACyT.

Institutional Review Board Statement: Not applicable.

Informed Consent Statement: Not applicable.

Data Availability Statement: Data will be supplied on reasonable request by emailing K.M.

Conflicts of Interest: The authors declare no conflict of interest.

Abbreviations

The following abbreviations are used in this manuscript:

CO_2	Carbon dioxide.
DNA	Deoxyribonucleic acid.
HCN	Hydrogen cyanide.
H_2S	Hydrogen sulfide.
RNA	Ribonucleic acid.
UV-A	Light in the region 360–400 nm.
UV-B	Light in the region 285–360 nm.
UV-C	Light in the region 100–285 nm (only the region 180–285 nm is relevant here since shorter wavelengths are well shielded by atmospheric CO_2).
UVTAR	Ultraviolet and Temperature-Assisted Replication.

References

1. Fan, Y.; Fang, Y.; Ma, L. The self-crosslinked ufasome of conjugated linoleic acid: Investigation of morphology, bilayer membrane and stability. *Colloids Surf. B Biointerfaces* **2014**, *123*, 8–14. [CrossRef] [PubMed]
2. Deamer, D. The Role of Lipid Membranes in Life's Origin. *Life* **2017**, *7*, 5. [CrossRef] [PubMed]
3. Saha, A.; Yi, R.; Fahrenbach, A.C.; Wang, A.; Jia, T.Z. A Physicochemical Consideration of Prebiotic Microenvironments for Self-Assembly and Prebiotic Chemistry. *Life* **2022**, *12*, 1595. [CrossRef]
4. Gözen, I.; Köksal, E.S.; Põldsalu, I.; Xue, L.; Spustova, K.; Pedrueza-Villalmanzo, E.; Ryskulov, R.; Meng, F.; Jesorka, A. Protocells: Milestones and Recent Advances. *Small* **2022**, *18*, 2106624. [CrossRef]
5. Michaelian, K. The Dissipative Photochemical Origin of Life: UVC Abiogenesis of Adenine. *Entropy* **2021**, *23*, 217. [CrossRef]
6. Hernández, C.; Michaelian, K. Dissipative Photochemical Abiogenesis of the Purines. *Entropy* **2022**, *24*, 1027. [CrossRef]
7. Lopez, A.; Fiore, M. Investigating Prebiotic Protocells for a Comprehensive Understanding of the Origins of Life: A Prebiotic Systems Chemistry Perspective. *Life* **2019**, *9*, 49. [CrossRef]
8. Ferris, J.P.; Orgel, L.E. An Unusual Photochemical Rearrangement in the Synthesis of Adenine from Hydrogen Cyanide. *J. Am. Chem. Soc.* **1966**, *88*, 1074. [CrossRef]
9. Barks, H.L.; Buckley, R.; Grieves, G.A.; Di Mauro, E.; Hud, N.V.; Orlando, T.M. Guanine, Adenine, and Hypoxanthine Production in UV-Irradiated Formamide Solutions: Relaxation of the Requirements for Prebiotic Purine Nucleobase Formation. *ChemBioChem* **2010**, *11*, 1240–1243. [CrossRef]
10. Sagan, C. Ultraviolet Selection Pressure on the Earliest Organisms. *J. Theor. Biol.* **1973**, *39*, 195–200. [CrossRef]
11. Mulkidjanian, A.Y.; Cherepanov, D.A.; Galperin, M.Y. Survival of the fittest before the beginning of life: Selection of the first oligonucleotide-like polymers by UV light. *BMC Evol. Biol.* **2003**, *3*, 12. [CrossRef] [PubMed]
12. Michaelian, K. Thermodynamic origin of life. *arXiv* **2009**, arXiv:0907.0042v3.
13. Michaelian, K. Thermodynamic dissipation theory for the origin of life. *Earth Syst. Dynam.* **2011**, *224*, 37–51. [CrossRef]
14. Michaelian, K.; Simeonov, A. Fundamental molecules of life are pigments which arose and co-evolved as a response to the thermodynamic imperative of dissipating the prevailing solar spectrum. *Biogeosciences* **2015**, *12*, 4913–4937. [CrossRef]
15. Michaelian, K. *Thermodynamic Dissipation Theory of the Origina and Evolution of Life: Salient Characteristics of RNA and DNA and Other Fundamental Molecules Suggest an Origin of Life Driven by UV-C Light*; Self-Published; CreateSpace: Mexico City, Mexico, 2016; ISBN 9781541317482.
16. Michaelian, K. Microscopic Dissipative Structuring and Proliferation at the Origin of Life. *Heliyon* **2017**, *3*, e00424. [CrossRef]
17. Schirrmeister, B.E.; Sanchez-Baracaldo, P.; Wacey, D. Cyanobacterial evolution during the Precambrian. *Int. J. Astrobiol.* **2016**, *15*, 187–204. [CrossRef]

18. Michaelian, K. Homochirality through Photon-Induced Denaturing of RNA/DNA at the Origin of Life. *Life* **2018**, *8*, 21. [CrossRef]
19. Michaelian, K.; Santillan, N. UVC photon-induced denaturing of DNA: A possible dissipative route to Archean enzyme-less replication. *Heliyon* **2019**, *5*, e01902. [CrossRef] [PubMed]
20. Glansdorff, P.; Prigogine, I. *Thermodynamic Theory of Structure, Stability and Fluctuations*; Wiley Interscience: Hoboken, NJ, USA, 1971.
21. Michaelian, K.; Rodriguez, O. Prebiotic fatty acid vesicles through photochemical dissipative structuring. *Rev. Cuba. QuíMica* **2019**, *31*, 354–370.
22. Cnossen, I.; Sanz-Forcada, J.; Favata, F.; Witasse, O.; Zegers, T.; Arnold, N.F. The habitat of early life: Solar X-ray and UV radiation at Earth's surface 4–3.5 billion years ago. *J. Geophys. Res.* **2007**, *112*, E02008. [CrossRef]
23. Michaelian, K. Non-Equilibrium Thermodynamic Foundations of the Origin of Life. *Foundations* **2022**, *2*, 308–337. [CrossRef]
24. Mulkidjanian, A.Y.; Bychkov, A.Y.; Dibrova, D.V.; Galperin, M.Y.; Koonin, E.V. Origin of first cells at terrestrial, anoxic geothermal fields. *Proc. Natl. Acad. Sci. USA* **2012**, *109*, E821–E830. [CrossRef] [PubMed]
25. Van Kranendonk, M.J.; Deamer, D.W.; Djokic, T. Life Springs. *Sci. Am.* **2017**, *317*, 28–35. [CrossRef] [PubMed]
26. Damer, B.; Deamer, D. The Hot Spring Hypothesis for an Origin of Life. *Astrobiology* **2020**, *20*, 429–452. [CrossRef] [PubMed]
27. Johnson, D. A synthesis of unsaturated very long chain fatty acids. *Chem. Phys. Lipids* **1990**, *56*, 65–71. [CrossRef]
28. Pereto, J.; Lopez-Garcia, P.; Moreira, D. Ancestral lipid biosynthesis and early membrane evolution. *Trends Biochem. Sci.* **2004**, *29*, 469–477. [CrossRef]
29. Lombard, J.; López-García, P.; Moreira, D. The early evolution of lipid membranes and the three domains of life. *Nat. Rev. Microbiol.* **2012**, *10*, 507–515. [CrossRef]
30. Knauth, L.P.; Lowe, D.R. High Archean climatic temperature inferred from oxygen isotope geochemistry of cherts in the 3.5 Ga Swaziland group, South Africa. *Geol. Soc. Am. Bull.* **2003**, *115*, 566–580. [CrossRef]
31. Knauth, L.P. Temperature and salinity history of the Precambrian ocean: implications for the course of microbial evolution. *Paleogeogr. Paleoclimatol. Paleoecol.* **2005**, *219*, 53–69. [CrossRef]
32. Meixnerová, J.; Blum, J.D.; Johnson, M.W.; Stüeken, E.E.; Kipp, M.A.; Anbar, A.D.; Buick, R. Mercury abundance and isotopic composition indicate subaerial volcanism prior to the end-Archean "whiff" of oxygen. *Proc. Natl. Acad. Sci. USA* **2021**, *118*, e2107511118. [CrossRef]
33. Han, J.; Calvin, M. Occurrence of fatty acids and aliphatic hydrocarbons in a 3.4 billion-year-old sediment. *Nature* **1969**, *224*, 576–577. [CrossRef] [PubMed]
34. Van Hoeven, W.; Maxwell, J.; Calvin, M. Fatty acids and hydrocarbons as evidence of life processes in ancient sediments and crude oils. *Geochim. Cosmochim. Acta* **1969**, *33*, 877–881. [CrossRef]
35. Rossignol, S.; Tinel, L.; Bianco, A.; Passananti, M. Atmospheric photochemistry at a fatty acid–coated air-water interface. *Science* **2016**, *353*, 699–702. [CrossRef] [PubMed]
36. Bowman, C.N.; Kloxin, C.J. Toward an enhanced understanding and implementation of photopolymerization reactions. *AIChE J.* **2008**, *54*, 2775–2795. [CrossRef]
37. Botta, L.; Bizzarri, B.M.; Piccinino, D.; Fornaro, T.; Brucato, J.R.; Saladino, R. Prebiotic synthesis of carboxylic acids, amino acids and nucleic acid bases from formamide under photochemical conditions. *Eur. Phys. J. Plus* **2017**, *132*, 317. [CrossRef]
38. Vicente, A.; Antunes, R.; Almeida, D.; Franco, I.J.A.; Hoffmann, S.V.; Mason, N.J.; Eden, S.; Duflot, D.; Canneaux, S.; Delwiche, J.; et al. Photoabsorption measurements and theoretical calculations of the electronic state spectroscopy of propionic, butyric, and valeric acids. *Phys. Chem. Chem. Phys.* **2009**, *11*, 5729–5741. [CrossRef]
39. Mandal, T.K.; Chatterjee, S.N. Ultraviolet- and Sunlight-Induced Lipid Peroxidation in Liposomal Membrane. *Radiat. Res.* **1980**, *83*, 290–302. [CrossRef]
40. Celani, P.; Garavelli, M.; Ottani, S.; Bemardi, F.; Robb, M.A.; Olivucci, M. Molecular "Trigger" for Radiationless Deactivation of Photoexcited Conjugated Hydrocarbons. *J. Am. Chem. Soc.* **1995**, *117*, 11584–11585. [CrossRef]
41. Bassas, M.; Marqués, A.M.; Manresa, A. Study of the crosslinking reaction (natural and UV induced) in polyunsaturated PHA from linseed oil. *Biochem. Eng. J.* **2007**, *40*, 275–283. [CrossRef]
42. Fan, Y.; Ma, J.; Fang, Y.; Liu, T.; Hu, X.; Xia, Y. Neutral and acid-adapted fatty acid vesicles of conjugated linoleic acid. *Colloids Surfaces B Biointerfaces* **2018**, *167*, 385–391. [CrossRef]
43. Milshteyn, D.; Damer, B.; Havig, J.; Deamer, D. Amphiphilic Compounds Assemble into Membranous Vesicles in Hydrothermal Hot Spring Water but Not in Seawater. *Life* **2018**, *8*, 11. [CrossRef] [PubMed]
44. Martin, N.; Douliez, J.P. Fatty Acid Vesicles and Coacervates as Model Prebiotic Protocells. *ChemSystemsChem* **2021**, *3*, e2100024. [CrossRef]
45. Fan, Y.; Fang, Y.; Ma, L.; Jiang, H. Investigation of Micellization and Vesiculation of Conjugated Linoleic Acid by Means of Self-Assembling and Self-Crosslinking. *J. Surfact. Deterg.* **2015**, *18*, 179–188. [CrossRef]
46. Carballeira, N.; Sostre, A.; Stefanov, K.; Popov, S.; Kujumgiev, A.; Dimitrova-Konaklieva, S.; Tosteson, C.; Tosteson, T. The fatty acid composition of a Vibrio alginolyticus associated with the alga Cladophora coelothrix. Identification of the novel 9-methyl-10-hexadecenoic acid. *Lipids* **1997**, *32*, 1271–1275. [CrossRef]
47. Hippchen, B.; Röll, A.; Poralla, K. Occurrence in soil of thermo-acidophilic bacilli possessing ω-cyclohexane fatty acids and hopanoids. *Arch. Microbiol.* **1981**, *129*, 53–55. [CrossRef]

48. Talrose, V.; Yermakov, A.N.; Usov, A.A.; Goncharova, A.A.; Leskin, A.N.; Messineva, N.A.; Trusova, N.V.; Efimkina, M.V. *NIST Chemistry WebBook*; National Institute of Standards and Technology: Gaithersburg, MD, USA, 2023; Chapter UV/Visible Spectra, in NIST Standard Reference Database Number 69.
49. Bohren, C.F.; Huffman, D.R. *Absorption and Scattering of Light by Small Particles*; Wiley: New York, NY, USA, 1998.
50. Hale, G.M.; Querry, M.R. Optical Constants of Water in the 200-nm to 200-µm Wavelength Region. *Appl. Opt.* **1973**, *12*, 555–563. [CrossRef]
51. Bertolotto, J.; Reale, M.P.; Rodriguez, M.B. DETERMINACIÓN DEL TENSOR POLARIZABILIDAD ÓPTICA DEL ADN TIPO VARILLA. *Anales AFA* **2013**, *11* , 302–306.
52. Liu, P.Y.; Chin, L.K.; Ser, W.; Chen, H.F.; Hsieh, C.M.; Lee, C.H.; Sung, K.B.; Ayi, T.C.; Yap, P.H.; Liedberg, B.; et al. Cell refractive index for cell biology and disease diagnosis: Past, present and future. *Lab Chip* **2016**, *16*, 634–644. [CrossRef]
53. Gardiner, C.; Shaw, M.; Hole, P.; Smith, J.; Tannetta, D.; Redman, C.W.; Sargent, I.L. Measurement of refractive index by nanoparticle tracking analysis reveals heterogeneity in extracellular vesicles. *J. Extracell. Vesicles* **2014**, *3*, 25361. [CrossRef]
54. Xu, S.; Li, X. Refractive index characteristics of edible oils based on spectrometry and effects of oil dispersion on OCT. *J. Innov. Opt. Health Sci.* **2021**, *14*, 2140010. [CrossRef]
55. Chaplin, M. Water Structure and Science. 2016. Available online: https://water.lsbu.ac.uk/water (accessed on 22 February 2023).
56. Umazano, J.; Bertolotto, J. Optical properties of DNA in aqueous solution. *J. Biol. Phys.* **2008**, *34*, 163–177. [CrossRef] [PubMed]
57. Wolstencroft, R.D. Terrestrial and Astronomical Sources of Circular Polarisation: A Fresh Look at the Origin of OF Homochirality on Earth. *Proc. Int. Astron. Union* **2004**, *213*, 154. [CrossRef]
58. Michaelian, K. Thermodynamic stability of ecosystems. *J. Theor. Biol.* **2005**, *237*, 323–335. [CrossRef] [PubMed]